Atmos. Chem. Phys. Discuss., 13, 24713–24754, 2013
www.atmos-chem-phys-discuss.net/13/24713/2013/
doi:10.5194/acpd-13-24713-2013

Atmospheric Chemistry and Physics Discussions
Open Access

Role of ozone in SOA formation from alkane photooxidation

X. Zhang[1], R. H. Schwantes[1], M. M. Coggon[2], C. L. Loza[2], K. A. Schilling[2], R. C. Flagan[1,2], and J. H. Seinfeld[1,2]

[1]Division of Engineering and Applied Science, California Institute of Technology, Pasadena, CA, USA
[2]Division of Chemistry and Chemical Engineering, California Institute of Technology, Pasadena, CA, USA

Received: 15 August 2013 – Accepted: 4 September 2013 – Published: 24 September 2013

Correspondence to: J. H. Seinfeld (seinfeld@caltech.edu)

Published by Copernicus Publications on behalf of the European Geosciences Union.

Abstract

Long-chain alkanes, which can be categorized as intermediate volatile organic compounds (IVOCs), are an important source of secondary organic aerosol (SOA). Mechanisms for the gas-phase OH-initiated oxidation of long-chain alkanes have been well documented; particle-phase chemistry, however, has received less attention. The δ-hydroxycarbonyl, which is generated from the isomerization of alkoxy radicals, can undergo heterogeneous cyclization to form substituted dihydrofuran. Due to the presence of C=C bonds, the substituted dihydrofuran is predicted to be highly reactive with OH, and even more so with O_3 and NO_3, thus opening a reaction pathway that is not usually accessible to alkanes. This work focuses on the role of substituted dihydrofuran formation and its subsequent reaction with OH, and more importantly ozone, in SOA formation from the photooxidation of long-chain alkanes. Experiments were carried out in the Caltech Environmental Chamber using dodecane as a representative alkane to investigate the difference in aerosol composition generated from "OH-oxidation dominating" vs. "ozonolysis dominating" environments. A detailed mechanism incorporating the specific gas-phase photochemistry, together with the heterogeneous formation of substituted dihydrofuran and its subsequent gas-phase OH/O_3 oxidation, is presented to evaluate the importance of this reaction channel in the dodecane SOA formation. We conclude that: (1) the formation of δ-hydroxycarbonyl and its subsequent heterogeneous conversion to substituted dihydrofuran is significant in the presence of NO_x; (2) the ozonolysis of substituted dihydrofuran dominates over the OH-initiated oxidation under conditions prevalent in urban and rural air; and (3) a spectrum of highly-oxygenated products with carboxylic acid, ester, and ether functional groups are produced from the substituted dihydrofuran chemistry, thereby affecting the average oxidation state of the SOA.

ACPD
13, 24713–24754, 2013

1 Introduction

Alkanes are important constitutents of gasoline and vehicle emissions (Hoekman, 1992; Zielinska et al., 1996; Kirchstetter et al., 1999), accounting for ~ 50 % of volatile organic compounds (VOCs) in the urban atmosphere (Fraser et al., 1997; Schauer et al., 1999 and 2002). The unresolved complex mixture (UCM) of organics, which is potentially a significant source of secondary organic aerosol (SOA) formation in the atmosphere, has recently been shown to comprise many long-chain alkanes (Isaacman et al., 2012), which are expected to contribute SOA formation (Robinson et al., 2007).

Laboratory chamber investigations of SOA formation from long-chain alkanes (Lim and Ziemann, 2005, 2009a, b, c; Presto et al., 2009, 2010; Miracolo et al., 2010, 2011; Craven et al., 2012; Lambe et al., 2012; Tkacik et al., 2012; Yee et al., 2012; Loza et al., 2013) provide a framework for understanding chemical mechanisms and determination of SOA yields (Jordan et al., 2008; Aumont et al., 2012, 2013; Cappa et al., 2012; Zhang and Seinfeld, 2013). Particle-phase products from OH oxidation of alkanes contain a number of functional groups: organonitrate ($-ONO_2$), hydroxyl (−OH), carbonyl (−C=O), ester (-C(O)O-), and hydroxyperoxide (−OOH). Ambient measurements of organic aerosol composition have shown, in addition, that the carboxylic acid functional group (−C(O)OH) is closely associated with products from fossil fuel combustion sources (Liu et al., 2011; Russell et al., 2011), of which alkanes are a principal component.

Atmospheric alkanes react in daytime exclusively with OH, producing an array of peroxy radicals (RO_2). In the presence of sufficient NO, the alkoxy radical (RO) is the key product of the subsequent RO_2 reaction with NO. $RONO_2$ is also produced, with a branching ratio of 0.1–0.3 (Arey et al., 2001). For alkanes with carbon number ≥ 5, the 1, 5-H shift isomerization is the dominant reaction pathway for RO, producing a δ-hydroxycarbonyl, the primary fate of which is reaction with OH (Jenkin et al., 2003; Saunders et al., 2003; Bloss et al., 2005), with a lifetime of ~ 11.5 h at room temperature and a typical ambient OH concentration of 1×10^6 molecules cm^{-3}. One

ACPD
13, 24713–24754, 2013

particular δ-hydroxycarbonyl, 5-hydroxy-2-pentanone, was found to cyclize to form the cyclic hemiacetal. The cyclic hemiacetal can subsequently lose water to form 4, 5-dihydro-2-methylfuran, with an overall lifetime as short as ~ 1.1 h at 298 K (Cavalli et al., 2000; Martin et al., 2002). The presence of water vapor can, in principle, serve to convert the 4, 5-dihydro-2-methylfuran back to 5-hydroxy-2-pentanone, leading to an equilibrium between these two species within several hours (Martin et al., 2002; Baker et al., 2005; Holt et al., 2005; Reisen et al., 2005).

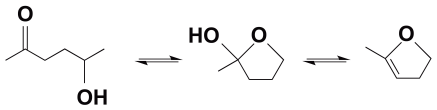

This conversion to 4,5-dihydro-2-methylfuran is not unique to 5-hydroxy-2-pentanone but also occurs for other C_5-C_{17} δ-hydroxycarbonyls (Lim and Ziemann, 2005, 2009a, b, c), at a rate that increases with the length of the carbon chain (Holt et al., 2005; Ziemann and Atkinson, 2012). The substituted dihydrofuran is highly reactive towards OH, O_3, and NO_3 in the gas phase, owing to the presence of a C=C double bond. For typical ambient concentrations of OH, O_3, and NO_3, i.e., 2×10^6 moleculescm^{-3} (12 h average), 30 ppb (24 h average), and 5×10^8 moleculescm^{-3} (12 h average), respectively, the lifetimes of the substituted dihydrofuran with respect to reactions with these oxidants in the gas phase are 1.3 h, 7 min, and 24 s, respectively (Martin et al., 2002; Ziemann and Atkinson, 2012). Based on these estimates, ozonolysis of substituted dihydrofurans may dominate OH oxidation during daytime in the urban atmosphere.

SOA formation from long-chain alkanes involves multiple generations of OH oxidation that involve functionalization (O-atom addition in forms of a variety of moieties) and fragmentation of the parent carbon backbone. These two classes of processes eventually lead to highly oxygenated fragments that partition into the particle phase. Two recent modeling studies of C_{12} alkanes suggested that particle-phase chemistry might play a potentially important role in the chemical composition of alkane SOA; this

ACPD
13, 24713–24754, 2013

is inferred from the fact that simulations driven solely by gas-phase chemistry can successfully reproduce the chamber measured SOA yield, but these fail to reproduce the observed particulate O : C and H : C ratios in the absence of a particle-phase chemistry channel (Cappa et al., 2012; Zhang and Seinfeld, 2013). The extent to which particle-phase chemistry is important in alkane SOA formation has not been clearly established.

We address here the heterogeneous formation of substituted dihydrofurans and their subsequent gas-phase reaction with ozone in SOA formation from alkanes. We present the results of a series of chamber dodecane photooxidation experiments under two reaction regimes, i.e., "OH-dominant", in which over 70 % of substituted dihydrofurans are oxidized by OH, vs. "O_3-dominant", in which 80–90 % of substituted dihydrofurans react with O_3. Gas-phase products that are unique to the substituted dihydrofuran chemistry are identified. The impact of ozonolysis of substituted dihydrofurans on the particle-phase product distribution from the photooxidation of dodecane is investigated by comparing intensities of certain ions that are indicative of ozonolysis chemistry. We also develop a detailed mechanism with the incorporation of substituted dihydrofuran chemistry and simulate the effect of this reaction channel on SOA yield from the photooxidation of dodecane.

2 Experimental

Experiments were conducted in the new Caltech dual 24 m^3 Environmental Chamber, in which the temperature (T) and relative humidity (RH) are automatically controlled. Prior to each experiment, the Teflon chambers were flushed with clean, dry air for 24 h until the particle number concentration $< 10\,cm^{-3}$ and volume concentration $< 0.1\,\mu m^3\,cm^{-3}$. Seed aerosol was injected into the chamber by atomizing 0.015 M aqueous ammonium sulfate solution to provide sufficient surface area for the partition of semi-volatile products. Hydrogen peroxide (H_2O_2) was used for the OH source by evaporating 85 and 226 µL of 50 % wt aqueous solution into the chamber with 5 L min^{-1}

ACPD
13, 24713–24754, 2013

of purified air for ~ 110 min, resulting in an approximate starting H_2O_2 concentration of 1.5 and 4 ppm, respectively, under high- and low-NO_x conditions. The 4 ppm H_2O_2 concentration employed in low-NO_x experiments creates a $RO_2 + HO_2$ dominant reaction regime. Nitrous acid (HONO) replaced H_2O_2 as the OH source for one experiment in order to minimize the formation of ozone. HONO was prepared by dropwise addition of 15 mL of 1 wt% $NaNO_2$ into 30 mL of 10 wt% H_2SO_4 in a glass bulb and introduced into the chambers with 5 L min^{-1} of purified air for ~ 40 min. To minimize the vapor phase wall loss along the injection line, 60 µL of dodecane (Sigma-Aldrich, 98 % purity) was injected into a glass bulb, which was connected directly into the Teflon chamber via a 1/4″ I.D. Swagelock to NPT fitting located on a Teflon plate. Heated 5 L min^{-1} of purified air flowed through the glass bulb into the chamber for 30 min, introducing ~ 20 ppb dodecane into the chamber. After ~ 1 h mixing, photooxidation was initiated by irradiating the chamber with black lights with output wavelength ranging from 300 to 400 nm.

Experiments were carried out under conditions in which the peroxy radicals formed from the initial OH reaction with dodecane react either essentially exclusively with NO (so-called high-NO_x) (Exp. #1, #2, #3, #4, and #5) or essentially exclusively with HO_2 (so-called low-NO_x) (Exp. #6, #7, and #8). For each condition, "O_3-dominant" vs. "OH-dominant" environments were generated by varying the OH source, initial NO, NO_2, and O_3 concentrations, and the additional NO injection rate during the irradiation period (Table 1). The ozonolysis vs. OH oxidation of substituted dihydrofuran is calculated to be equally competitive when the ratio of O_3 to OH concentration is $6.3 \times 10^4 : 1$ (approximately 2.6 ppb O_3 vs. 1.0×10^6 molecule cm^{-3} OH). Under low-NO_x conditions, NO, NO_2, NO_x, and O_3 were below detection limits and no ozone formation was observed over the course of 20 h experiments. OH-oxidation of dihydrofuran is dominant with average OH concentrations of 1.8×10^6 and 1.5×10^6 molecule cm^{-3}, respectively, in Exp. #6 and #8. OH concentration is calculated by optimal fitting of the exponential decay of the GC-FID measured dodecane temporal profile. In order to evaluate the effect of the ozonolysis of dihydrofuran chemistry on the dodecane SOA formation under

ACPD
13, 24713–24754, 2013

low-NO_x conditions, additional ~ 30 ppb of ozone was injected into the chamber before the onset of irradiation (Exp. #7). Under high-NO_x conditions, HONO was used as the OH source for the "OH dominant" environment (Exp. #1). Double HONO injection was carried out in order to fully consume dodecane (before the onset and after ~ 3 h of irradiation). The average OH concentration is ~ 5.0×10^6 molecule cm^{-3}, whereas O_3 peaks at 8 ppb after 60 min of photooxidation and rapidly decays to ~ 0 ppb within 2 h. In this case, > 73 % of dihydrofuran is oxidized by OH over the course of Exp. #1. An "O_3 dominant" environment was generated by injecting NO (38–287 ppb) and NO_2 (12–156 ppb) before the onset of irradiation. Continuous NO injection with a certain flow rate (20–100 ppb h^{-1}) was conducted over the course of experiments to reach a sufficient amount of O_3 and to maintain high-NO_x levels. Under experimental conditions in Exp. #2, #3, #4, and #5, the average OH concentrations are calculated to be 1.7×10^6, 2.0×10^6, 1.4×10^6, and 1.3×10^6 molecule cm^{-3}, respectively, and the maximum O_3 concentrations are 20, 380, 150, and 250 ppb, respectively. As a result, ~ 82 %, ~ 96 %, ~ 97 %, and ~ 98 % of dihydrofuran reacts with O_3 when dihydrofuran peaks after ~ 3 h of photooxidation. High humidity experiments were also carried out as a set of control experiments (Exp. #4, #5, and #8) considering the role of water vapor in the heterogeneous interconversion between δ-hydroxycarbonyls and substituted dihydrofurans.

A suite of instruments was used to investigate gas- and particle-phase chemistry. T, RH, NO, NO_x, and O_3 were continuously monitored. Dodecane concentration was monitored by taking hourly samples at ~ 0.13 L min^{-1} of chamber air for 3 min onto a Tenax adsorbent, which was loaded into the inlet of a gas chromatograph with flame ionization detection (GC/FID, Agilent 6890N), desorbed at 275 °C for 13 min, and then injected onto an HP-5 column (15 m × 0.53 mm ID × 1.5 µm thickness, Hewlett-Packard) held at 30 °C. The oven was ramped from 30 to 275 °C at 10 °C min^{-1} and held at 275 °C for 5 min. The retention time for dodecane is ~ 27.5 min. The gas-phase species were monitored using a custom-modified Varian 1200 triple-quadrupole chemical ionization mass spectrometer (CIMS) (Crounse et al., 2006; Paulot et al., 2009). In negative mode

ACPD
13, 24713–24754, 2013

operation, CF_3O^- was used as the reagent ion to cluster with an analyte such as hydroperoxide or acid [R], producing $[R{\cdot}CF_3O]^-$ or m/z $[M+85]^-$, where M is the molecular weight of the analyte. For more strongly acidic species [H·X], the transfer product, $[H{\cdot}X{\cdot}F]^-$ or m/z $[M+19]^-$, is formed during ionization. Carboxylic acids tend to have contributions to both the transfer and cluster product, in which case the overall signal of a compound is considered as the sum of the two product signals. In positive mode operation, an analyte [R] can undergo proton transfer reaction, producing an ion in the form of $[R{\cdot}H]^+$, and/or react with n positively charged water clusters to form a cluster in the form of $[(H_2O)_n{\cdot}R{\cdot}H]^+$. Positive mode is employed in this study for tracking less polar compounds, such as the substituted dihydrofuran.

Particle size distribution and number concentration were measured by a cylindrical differential mobility analyzer (DMA; TSI Model 3081) coupled to a condensation particle counter (TSI Model 3010). The protocol for applying wall loss correction to DMA measured SOA growth data is described in the Supplement. Real-time particle mass spectra were collected continuously by an Aerodyne High Resolution Time-of-Flight Aerosol Mass Spectrometer (DeCarlo et al., 2006; Canagaratna et al., 2007). The AMS switched once every minute between the high resolution "W-mode" and the lower resolution, higher sensitivity "V-mode". The V-mode was utilized for quantification, as the higher m/z values exhibit a more favorable signal-to-noise ratio. The W-mode was used for ion identification and clarification. Detailed AMS data analysis protocols can be found in the Supplement.

3 Chemical mechanism

A photochemical mechanism was used to simulate the gas-phase photochemistry of NO_x, HO_x, and O_3 corresponding to the experimental conditions. Reactions and corresponding reaction rate constants are listed in Tables S1–3 in Supplement. Photolysis rate constants are calculated using the irradiance spectrum measured for the chamber UV lights, and absorption cross sections and quantum yields from Sander et al. (2011).

ACPD
13, 24713–24754, 2013

The kinetic scheme for the gas-phase OH-initiated oxidation of dodecane and the further OH oxidation of multi-generational products was developed primarily based on the MCMv3.2 (http://mcm.leeds.ac.uk/MCM/). Products identified in Lim and Ziemann (2005, 2009a, b, c) that are not in MCM are also included here. The kinetic scheme was incorporated in the photochemical model to estimate yields of particle-phase products generated in the chamber. A simplified flow chart illustrating the mechanism for the multi-generation gas-phase chemistry is shown in Fig. 1a, b. In general, the OH-initiated oxidation of dodecane leads to RO_2, the fate of which controls the distribution of further generation products. When sufficient NO_x is present (the concentration of NO, i.e., > 5 ppb, is at least four orders of magnitude higher than RO_2, i.e., $< 5 \times 10^7$ molecules cm^{-3}), over 99 % of RO_2 reacts with NO, leading to RO or alkyl nitrate ($RONO_2$). The branching ratios for the production of RO and $RONO_2$ are obtained from Jordan et al. (2008). RO can isomerize through a 1,5 H-atom shift to a δ-hydroxyalkyl radical, react with O_2, or undergo fragmentation. The alkyl nitrate formed either undergoes photolysis or reacts with OH via H-atom abstraction from a C-atom or reacts with OH via H-atom abstraction from a C-atom with a $-ONO_2$ group attached to produce a –C=O group. The δ-hydroxyalkyl radical reacts with O_2 and then NO and undergoes another isomerization to produce a δ-hydroxycarbonyl. At sufficiently low NO_x concentrations, the simulated HO_2 concentration ($\sim 1 \times 10^{10}$ molecules cm^{-3}) is $\sim$ 20 times higher than RO_2 ($\sim 5 \times 10^8$ molecules cm^{-3}). $RO_2 + HO_2$ dominates the fate of RO_2, producing a hydroperoxide (ROOH). Further oxidation of ROOH involves the photolysis of the –OOH group, H-atom abstraction, and the OH oxidation of a C-atom with a –OOH group attached to produce a –C=O group. Products through eight generations of oxidation are included in the mechanism, although only the formation of the first three generations of products is illustrated in Fig. 1. The reaction rate constants are obtained from MCM v3.2. In the absence of specific data, the photolysis rate constants of the –OOH, –C=O, and $-ONO_2$ groups on the carbon backbone are assumed to be the same as those for methyl peroxide (CH_3OOH), 2-butanol (C_3H_7CHO), and *n*-propyl nitrate (n-CH_3ONO_2).

ACPD
13, 24713–24754, 2013

Cyclization and subsequent dehydration of δ-hydroxycarbonyl to substituted dihydrofuran is a heterogeneous process, including (1) gas-phase diffusion and reactive uptake of δ-hydroxycarbonyl to particles, (2) cyclization of δ-hydroxycarbonyl to cyclic hemiacetal, and (3) dehydration of cyclic hemiacetal to substituted dihydrofuran. (Atkinson et al., 2008; Lim and Ziemann, 2009c). The extent of this heterogeneous process occurring on/in particles has been recently predicted to predominate over chamber walls (Lim and Ziemann, 2009c). In this study, we represent the individual steps of the conversion of δ-hydroxycarbonyl to substituted dihydrofuran by an overall first-order decay rate of $3 \times 10^{-3}\,s^{-1}$. This value is estimated by monitoring the decay of 5-hydroxy-2-pentanone using CIMS in the presence of $20\,\mu m^3\,cm^{-3}$ NH_4HSO_4 seeds and 200 ppb O_3 at 3 % RH. This assumed decay rate is consistent with those measured in previous studies (Cavalli et al., 2000; Martin et al., 2002; Holt et al., 2005; Lim and Ziemann, 2009). The equilibrium constant K (K = (dihydrofuran)/(δ-hydroxycarbonyl)) is estimated to be ~ 7 at 3 % RH from the CIMS measured δ-hydroxycarbonyl decay curve, based on the assumption that the decrease in the δ-hydroxycarbonyl concentration is accompanied by a stoichiometric formation of the corresponding substituted dihydrofuran. Note that although the proportion of the heterogeneous conversion occurring on the chamber walls is unknown, the potential contribution of chamber walls to the particle-phase production of substituted dihydrofuran has been accounted by employing the measured overall conversion rate in the mechanism.

The substituted dihydrofuran formed evaporates rapidly due to its high volatility and undergoes reactions with OH, O_3, and NO_3 in the gas phase (Ziemann and Atkinson, 2012), with reaction rate constants of 2.18×10^{-10}, $3.49 \times 10^{-15}\,cm^3\,molecule^{-1}\,s^{-1}$, and $1.68 \times 10^{-10}\,cm^3\,molecule^{-1}\,s^{-1}$, respectively (Martin et al., 2002; Atkinson et al., 2008). Reaction with NO_3 is not important under the conditions of this study. In general, the OH addition to an alkyl-substituted dihydrofuran produces either an alkyl-substituted tetrahydrofuran or a carbonyl ester, see Fig. 2a (Martin et al., 2002; Lim and Ziemann, 2005, 2009a, b, and c; Jordan et al., 2008). The mechanism for the O_3 reaction with an alkyl-substituted dihydrofuran, as shown in Fig. 2b, was developed

ACPD
13, 24713–24754, 2013

following the ozonolysis of 4,5-dihydro-2-methylfuran (Martin et al., 2002), alkyl vinyl ethers (Thiault et al., 2002; Klotz et al., 2004; Sadezky et al., 2006) and monoterpenes (Jenkin et al., 2000; Jenkin, 2004). The reaction of alkyl-substituted dihydrofuran with O_3 involves the addition of O_3 to the C=C double bond to produce an energy-rich primary ozonide, which rapidly decomposes into two excited Criegee intermediates. The energy-rich Criegee intermediates are either collisionally stabilized, or decompose to yield OH (or OH + CO) and an additional α-carbonyl peroxy radical (or peroxy radical). The resulting α-carbonyl peroxy radical (or peroxy radical) can undergo the well-established reactions available for peroxy radicals, see Fig. 2b. The stabilized Criegee intermediates are predicted to react primarily with water (Martin et al., 2002), leading to 3-propoxy-nonanal ($C_{12}H_{22}O_3$) and 3-propoxy-nonanic acid ($C_{12}H_{22}O_3$), with molar yields of 90 % and 10 %, respectively. The total yield of 3-propoxy-nonanal is predicted to be 18 %, which is close to the yield of succinaldehydic acid methyl ester (23 %) from the ozonolysis of 4,5-dihydro-2-methylfuran (Martin et al., 2002).

We consider SOA formation by dodecane photooxidation, including heterogeneous formation of substituted dihydrofuran and its subsequent reaction with OH/O_3. Gas-particle equilibrium partitioning of semi-volatile products is assumed. The branching ratio and vapor pressure ($P_{L,i}$/atm) at 300 K (predicted by SIMPOL.1 (Pankow and Asher, 2008)) of each product from the OH/O_3 initiated oxidation of alkyl-substituted dihydrofuran are labeled in Fig. 2. The corresponding effective saturation concentrations ($C^* = 10^6 P^0_{L,i} \gamma_i \bar{M}_w / RT$) range from 7.0×10^1 µg m^{-3} to 4.7×10^4 µg m^3, for which approximately 0.1 % ~ 41.7 %, respectively, of these products are in the particle phase at an organic loading of ~ 50 µg m^{-3}. Compounds with the lowest volatility (~ 10^{-9} atm) are produced mostly from the $RO_2 + NO \rightarrow RONO_2$ reaction, the branching ratio of which ranges from 0.11 to 0.28. As a result, the total amount of organic nitrates in the particle-phase is relatively high, see Fig. 9c. Compounds generated from the $RO_2 + NO \rightarrow RO$ reaction have higher molar yields (0.72–0.89). But they are too volatile (~ 10^{-6}–10^{-7} atm) to partition significantly into the particle phase. The stabilized Criegee intermediate reaction with water is predicted to predominate over reaction with NO/NO_2

ACPD
13, 24713–24754, 2013

at RH > 3 %. The ester containing carboxylic acid ($C_{12}H_{22}O_4$) is predicted to be present in the particle phase due to its sufficiently low volatility (~ 10^{-8} atm), see Fig. 9d.

4 Results and discussion

In this section, we seek to evaluate the impact of substituted dihydrofuran chemistry on dodecane SOA formation as follows: (1) predict the yield of alkyl-substituted dihydrofuran from the photooxidation of dodecane under both high- and low-NO_x conditions, and the fraction of alkyl-substituted dihydrofuran that reacts with O_3 in the "O_3-dominant" regime (Sect. 4.1); (2) measure the time-dependent evolution of cyclic hemiacetal and alkyl-substituted dihydrofuran at 3 %, 10 %, 20 % and 50 % RH (Sect. 4.2); (3) propose gas-phase products that are unique to dihydrofuran chemistry based on the CIMS speciation (Sect. 4.3); (4) compare particle-phase chemical composition under "OH-dominant" vs. "O_3-dominant" environments via identifying AMS measured ions representative of dihydrofuran oxidation products (Sect. 4.4); and (5) estimate the change in SOA yield by incorporating the complete substituted-dihydrofuran formation and removal pathways into the dodecane SOA prediction model (Sect. 4.5).

4.1 Predicted substituted dihydrofuran formation and reaction with ozone in the dodecane system

To what extent is the formation of substituted dihydrofuran and its subsequent chemistry important in the formation of dodecane SOA? A mechanism simulation was conducted, with initial conditions similar to those employed in the chamber (Table 1), i.e., 200 ppb dodecane, 1.5 ppm H_2O_2, 100 ppb O_3, and 100 ppb + 30 ppb h^{-1} NO for high-NO_x conditions and 200 ppb dodecane, 4 ppm H_2O_2, 100 ppb O_3, and 0 ppb NO_x for low-NO_x conditions, respectively. Figure 3 shows the predicted mass distribution of δ-hydroxycarbonyl, alkyl-substituted dihydrofuran, together with other products of the same generation. δ-hydroxycarbonyl is predicted to account for > 90 % total organic

ACPD
13, 24713–24754, 2013

mass of first-generation products under high-NO_x conditions, see Fig. 3a (H). But it contributes < 5 % to the total organic mass of the third-generation products under low-NO_x conditions, see Fig. 3a (L). Inclusion of the heterogeneous conversion pathway from δ-hydroxycarbonyl to alkyl-substituted dihydrofuran is predicted to result in a rapid consumption of δ-hydroxycarbonyl under dry conditions, as opposed to a slow decay from OH oxidation. Alkyl-substituted dihydrofuran accounts for up to 70 % of the decay of δ-hydroxycarbonyl, as shown in Fig. 3b (H). As discussed earlier, an ozonolysis-dominant environment occurs for O_3 > 3 ppb at a typical OH concentration of 1.0×10^6 molecules cm^{-3}. In the high-NO_x simulation case, ozone is predicted to lead to 82–98 % of the total alkyl-substituted dihydrofuran loss over the course of photooxidation, see Fig. 3d (H).

The alkyl-substituted dihydrofuran is not the only product that contains a dihydrofuran structure in the dodecane photooxidation system. The first generation product, 3-dodecyl nitrate under high-NO_x conditions is an example. Three pathways exist that could produce semi-volatile compounds containing a dihydrofuran structure from the further photochemical reaction of 3-dodecyl nitrate: (1) photolysis of the $-ONO_2$ group leads to an alkyl-substituted dihydrofuran; (2) abstraction of an H-atom by OH potentially leads to an organonitrate-substituted dihydrofuran; and (3) H-atom abstraction from a C-atom with the $-ONO_2$ functional group attached and further H-atom abstraction from a C-atom potentially leads to a carbonyl-substituted dihydrofuran. It is worth noting that the gas-phase ozonolysis of alkyl-substituted dihydrofuran under high-NO_x conditions contributes to most of the ozonolysis reactions because the alkyl-substituted dihydrofuran is a major first-generation product, as shown in Fig. 3b (H).

4.2 Formation of cyclic hemiacetals and alkyl-substituted dihydrofuran

CIMS measurement at (+) m/z 183 in positive mode represents the ion $C_{12}H_{22}O{\cdot}H^+$ generated from the proton transfer reaction with alkyl-substituted dihydrofuran (M_w = 182). An additional source of (+) m/z 183 is the proton transfer reaction followed by dehydration of hydroxyl dodecanone (M_w = 200), which is also detected as a fluoride

ACPD
13, 24713–24754, 2013

cluster product at (−) m/z 285 ($C_{12}H_{24}O_2{\cdot}CF_3O^-$) in negative mode. Figure 4 shows temporal profiles of (+) m/z 183 and (−) m/z 285 monitored under both high- and low-NO_x conditions (Exp. 2 vs. Exp. 6). The (+) m/z 183 ion was detected in each of the two experiments, but with distinct time-dependent patterns. Under high NO_x-conditions, (+) m/z 183 peaks during first 3 h of irradiation, indicating fast formation of alkyl-substituted dihydrofuran, and decays during the next 15 h photooxidation. Under low-NO_x conditions, however, the (+) m/z 183 signal eventually reaches a plateau, which is more consistent with the pattern of (−) m/z 285. This behavior is consistent with the mechanism prediction that the alkyl-substituted dihydrofuran is formed in significant amounts only under high-NO_x conditions.

The AMS measured m/z 183 ($C_{12}H_{23}O^+$) is the major characteristic ion for cyclic hemiacetal. This ion is produced by the neutral loss of OH (M_w = 17) from the 2-position in the cyclic hemiacetal (M_w = 200) during electron ionization (Gong et al., 2005; Lim and Ziemann, 2009c). In addition, the $C_{12}H_{23}O^+$ ion is suggested to be the characteristic fragment of carbonyl-hydroperoxide-derived peroxyhemiacetal (Yee et al., 2012). The temporal profiles of the $C_{12}H_{23}O^+$ ion under both high- and low-NO_x conditions (Exp. 2 vs. Exp. 6) exhibit distinct growth patterns (Fig. 4). Under high-NO_x conditions, the $C_{12}H_{23}O^+$ ion signal increases rapidly to a maximum during the first 2 h and decays over the next ~ 14 h. The temporal behavior of the $C_{12}H_{23}O^+$ ion is a result of its rapid formation, i.e., uptake of δ-hydroxycarbonyl onto particles and subsequent cyclization, and relatively slower removal, i.e., dehydration. Under low-NO_x conditions, the $C_{12}H_{23}O^+$ ion increases over the course of a 20 h experiment because of the accumulative formation of peroxyhemiacetal. During the first 3 h of irradiation under low-NO_x conditions, the organic loading is below the AMS detection limit so that the $C_{12}H_{23}O^+$ ion signal does not appear in Fig. 4 during this period. The $C_{12}H_{23}O^+$ ion signal under low-NO_x conditions therefore potentially represents peroxyhemiacetal, since the formation of peroxides is the major reaction pathway in the RO_2+HO_2 dominant regime. This is again consistent with the mechanism prediction that the formation of alkyl-substituted dihydrofuran is unimportant under low-NO_x conditions.

ACPD
13, 24713–24754, 2013

Figure 5 shows temporal profiles of the ion $C_{12}H_{22}O{\cdot}H^+$ detected by CIMS and the ion $C_{12}H_{23}O^+$ detected by AMS in the presence of NO_x under varying RH. In general, the AMS ion $C_{12}H_{23}O^+$ peaks ~ 3 h earlier than the CIMS ion $C_{12}H_{22}O{\cdot}H^+$. The decay rates of AMS ion $C_{12}H_{23}O^+$, which is calculated by assuming first-order kinetics, are 4.02×10^{-3}, 3.06×10^{-3}, 1.71×10^{-3}, and $1.37 \times 10^{-3}\,s^{-1}$, respectively, at RH of 3 %, 10 %, 20 %, and 50 %. Aerosol water content could slow down the formation and removal rate of AMS ion $C_{12}H_{23}O^+$, mainly because: (1) water could accelerate the hydration rate, thus changing the equilibrium coefficient of the interconversion between cyclic hemiacetal and dihydrofuran; and (2) the addition of water might neutralize the particle-phase acid (e.g., HNO_3) which is thought to catalyze the cyclization of δ-hydroxycarbonyl to cyclic hemiacetal (Lim and Ziemann, 2009c). The decay rates of AMS ion $C_{12}H_{23}O^+$ are within the same order of magnitude of that measured for 5-hydroxy-2-pentanone at 3 % RH, indicating that the dehydration of cyclic hemiacetal is the rate-limiting step in the overall heterogeneous conversion process. Water vapor influences the sensitivity of the CIMS to certain compounds. The decreasing intensity of ion $C_{12}H_{22}O{\cdot}H^+$ as RH increases is likely indicative of this effect.

4.3 Products from alkyl-substituted dihydrofuran oxidation

Products unique to the alkyl-substituted dihydrofuran oxidation chemistry were proposed based on CIMS measured m/z signals, see Table 2 for chemical structures. Authentic standards are not commercially available for these products. Compounds from the dodecane photooxidation route that share the same m/z signal with alkyl-substituted dihydrofuran oxidation products are also presented in Table 2. The CIMS signal (−) m/z 346 is composed of 2-nitroxy-2-alkyl-3-hydroxyl-5-heptyl-tetrahydrofuran and 2-carbonyl-5-hydroxyl-2-dodecyl-nitrate. The latter is a 3rd generation product resulting from the further oxidation of dodecyl nitrate. The branching ratio for the addition of an $-ONO_2$ group is much lower than that for the formation of the RO radical, so that the interference of 2-carbonyl-5-hydroxyl-2-dodetyl-nitrate in the

ACPD
13, 24713–24754, 2013

(–) m/z 346 signal can be neglected. The CIMS signal (–) m/z 299 represents 3-propoxy-nonanal, which is a primary product from both OH-oxidation and ozonolysis of alkyl-substituted dihydrofuran, and 8-hydroxy-3,5-dodecanedione, which is produced from the further oxidation of dodecyl nitrate. As discussed earlier, the formation and transformation of dodecyl nitrate is predicted to be a minor pathway so that the (–) m/z 299 is dominated by 3-propoxy-nonanal.

A distinct feature of proposed products from the dihydrofuran oxidation by either OH or O_3 is the formation of an ester group (–C(O)O–) or an ether group (–O–), both of which can not be accessed from photochemical reaction pathways initiated by the OH attack on the aliphatic hydrocarbon. The OH oxidation channel leads solely to the formation of tetrahydrofuran and carbonyl ester. In the ozonolysis pathway, on the other hand, the reaction of stabilized Criegee intermediates with water produces one ester group containing aldehyde (3-propoxy-nonanal) and carboxylic acid (3-propoxy-nonanic acid); see proposed structures in Table 2. Due to the intact C_{12} skeleton and highly oxygenated nature, these two products are consistent with CIMS signals in (–) m/z 299 and (–) m/z 249 and 315 in negative mode with little interference from other products. Figure 6 shows the temporal profiles of (–) m/z 299, as well as (–) m/z 249 and 315, under "O_3 limiting" and "O_3 dominant" conditions. The decay rates of their precursor (+) m/z 183, as calculated by assuming first-order kinetics, are $1.44 \times 10^{-5}\,s^{-1}$ and $1.19 \times 10^{-5}\,s^{-1}$, respectively. Under "$O_3$ dominant" conditions, both species increase and eventually level off. When O_3 reaction is less competitive, the CIMS signals start to decrease after 10 h photooxidation.

4.4 Ozonolysis vs. OH-oxidation

Carboxylic acids produce significant signals at m/z 60 and 73, specifically $C_2H_4O_2^+$ and $C_3H_5O_2^+$, in the AMS measurement (Aiken et al., 2008). The formation of these two ions, as a function of the time-dependent decay of the ion $C_{12}H_{23}O^+$, is shown under different RH conditions in Fig. 7. The largest slope of either $\Delta C_2H_4O_2^+/\Delta C_{12}H_{23}O^+$ or

ACPD
13, 24713–24754, 2013

$\Delta C_3H_5O_2^+/\Delta C_{12}H_{23}O^+$ is associated with the highest RH, i.e., 50 %. On the contrary, the production of $C_2H_4O_2^+$ and $C_3H_5O_2^+$ is not significant under dry conditions. Also, the changes in slopes along with changes in RH values are consistent for both ions. This indicates that the formation of the carboxylic acid functional group detected in particles is associated with the water vapor concentration in the gas phase, consistent with the reaction of the stabilized Criegee intermediates with water in the substituted dihydrofuran oxidation system.

Two dominant oxygen-containing ions, m/z 44 (mostly CO_2^+) and m/z 43 ($C_3H_7^+$ and $C_2H_3O^+$), have been widely used to characterize organic aerosol evolution in chamber and field observations. Previous studies have shown that CO_2^+ results mostly from the thermal decarboxylation of an organic acid group (Alfarra, 2004). The f_{44} (ratio of m/z 43, mostly CO_2^+, to total signal in the component mass spectrum) axis is also considered to be an indicator of photochemical aging (Alfarra et al., 2004; Aiken et al., 2008; Kleinman et al., 2008). It has been found that increasing OH exposure increases f_{44} and decreases f_{43} (ratio of m/z 43, mostly $C_2H_3O^+$, to total signal in the component mass spectrum) for SOA generated from gas-phase alkanes (Lambe et al., 2011). The $C_2H_3O^+$ ion at m/z 43 is assumed predominantly due to non-acid oxygenates, such as saturated carbonyl groups (Ng et al., 2011). The evolution of dodecane SOA from four experiments (Table 1), characterized by different OH and O_3 exposure, and different RH levels, is shown in $f_{CO_2^+} - f_{C_2H_3O^+}$ space in Fig. 8. Overall, high-NO_x dodecane SOA lies to the lower left of the triangular region derived for ambient SOA. The relative high organic loading (~ 200 ppb dodecane) employed in this study favors partitioning of less oxidized species, which would remain in the gas phase under atmospheric conditions. For each experiment, $f_{CO_2^+}$ decreases and $f_{C_2H_3O^+}$ increases with increasing SOA at the beginning of irradiation. After several hours photooxidation, the trends reverse, resulting in increasing $f_{CO_2^+}$ and decreasing $f_{C_2H_3O^+}$. Curvature in $f_{CO_2^+} - f_{C_2H_3O^+}$ space has been also observed in other chamber/flow reactor studies (Kroll et al., 2009; Ng et al., 2010; Chhabra et al., 2011; Lee et al., 2011; Lambe et al., 2011).

ACPD
13, 24713–24754, 2013

As discussed in Sect. 2.1, Exp. #1 is designed as an "OH dominant" case, in which it is estimated that > 73 % of the dihydrofuran reacts with OH over the course of the experiment. Exp. #3, #4, and #5 were designed to be "O_3 dominant" at 10 %, 20 %, and 50 % RH, respectively. Approximately 96 %, 97 %, and 98 % of substituted dihydrofuran is predicted to react with O_3 when it peaks after ~ 3 h of photooxidation in Exp. #3, #4, and #5, respectively. As shown in Fig. 8, Exp. #1 exhibits the least intensity of $f_{CO_2^+}$ at the end of the experiment, i.e., 0.017, although the total OH exposure is the highest, i.e., 3.8×10^7 molecules cm^{-3} h. The total OH exposures for Exp. #3, 4, and 5 are 3.5 $\times$ 10^7, 2.2 $\times$ 10^7, and 2.1×10^7 molecules cm^{-3} h, respectively, which are less than that in Exp. #1. However, the intensities of $f_{CO_2^+}$ for these three experiments are 35–82 % higher than that in Exp. #1 at the end of experiments. In addition, the intensity of $f_{CO_2^+}$ increases along with increasing RH and O_3 exposure for these three experiments, varying from 0.023 to 0.031. The highest $f_{CO_2^+}$ intensity shown in Exp. #5 corresponds to the highest O_3 exposure and RH level, but lowest OH exposure.

The difference in chemical composition of organic particles produced from "O_3 dominant" vs. "OH dominant" environments is also examined via the time-dependent evolution of the average carbon oxidation state (OS_C) as calculated from AMS measured O : C and H : C ratios, see Fig. 9. Consistent with our findings in $f_{CO_2^+} - f_{C_2H_3O^+}$ space, the highest OS_C is observed under the highest O_3 exposure and RH level, but lowest OH exposure. With the same OH exposure, e.g., 1.5×10^7 molecules cm^{-3} h, the average carbon oxidation state increases from −1.36 to −1.25 under "O_3 limiting" (Exp. #1) vs. "O_3 dominant" environments (Exp. #5). One concludes that ozonolysis of substituted dihydrofuran plays an important role in the formation of highly oxidized aerosol in alkane SOA.

4.5 Experiment and model comparison

Figure 10a shows the simulated SOA growth (SIM.1) using the initial conditions in Exp. #2, together with the observed total organic aerosol mass as a function of reaction

ACPD
13, 24713–24754, 2013

time and OH exposure. The model reproduces the chamber measured SOA yield at 3 % RH when the conversion rate of $3 \times 10^{-3}\,s^{-1}$ is employed to represent the heterogeneous conversion of δ-hydroxycarbonyl to dihydrofuran. A second simulation (SIM.2) was run when the complete dihydrofuran chemistry was removed while other parameters were held constant. The total organic mass is ~ 42 % higher as a result after 18 h photooxidation. The formation of alkyl-substituted dihydrofuran from δ-hydroxycarbonyl is accompanied by an increase of vapor pressure from 5.36×10^{-7} to 1.08×10^{-4} atm at 300 K, as predicted by SIMPOL.1, and the total organic mass formed decreases. Although the addition of OH to the C=C double bond in the substituted dihydrofuran introduces an extra OH group, the decrease of vapor pressure owing to the addition of one OH group does not compensate for the heterogeneous conversion of both –C=O and –OH groups in δ-hydroxycarbonyl to an –O– group in a non-aromatic ring in dihydrofuran.

5 Atmospheric implications

The importance of ozone in the SOA formation from the photooxidation of long-chain alkanes under atmospherically relevant conditions depends on two factors: (1) the relative concentration of O_3 vs. OH; and (2) the heterogeneous conversion rate of δ-hydroxycarbonyls to substituted dihydrofurans. Figure 11 shows regimes of ozonolysis vs. OH-oxidation of substituted dihydrofuran corresponding to ranges of OH and O_3 concentrations. The OH-initiated oxidation of substituted dihydrofuran is predicted to dominate only under remote atmospheric conditions. Most alkane emissions occur in areas where ozone levels exceed 10 ppb, where the ozonolysis of dihydrofuran should be dominant.

Under conditions of the current study, the substituted dihydrofuran chemistry is predicted to account for > 95 % of the removal pathways of δ-hydroxycarbonyl (Fig. 3d (H)) and up to ~ 80 % of the total organic mass formed from dodecane photooxidation (Fig. 10b). This estimate sets the upper limit in terms of the contribution of substituted

ACPD
13, 24713–24754, 2013

dihydrofuran chemistry to alkane SOA production in the actual atmosphere, where the RH is higher (50 % vs. 3 %) and ambient organic aerosol levels are lower (~ 10 $\mu g\,m^{-3}$) than organic loadings in our chamber experiments (~ 50 $\mu g\,m^{-3}$ after 3 h of irradiation). Experimental evidence in this study shows that the heterogeneous conversion still occurs at 50 % RH but with less efficiency (Fig. 5). The water vapor abundance at 50 % RH, however, compensates for the production of the less substituted dihydrofuran, leading to an eventually higher yield of carboxylic acids (Sect. 4.4). If the conversion of δ-hydroxycarbonyl to substituted dihydrofuran occurs efficiently in the atmosphere, this could be a source of carboxylic acid in the ambient aerosols.

In summary, two impacts of substituted dihydrofuran chemistry on alkane SOA formation are expected. First, the SOA yield from the photooxidation of long-chain alkanes can be overpredicted without accounting for substituted dihydrofuran formation and removal pathways. Second, a substantial amount of carboxylic acid, ester, and tetrahydrofuran moieties can be produced, leading to higher O : C but much lower H : C ratios, and thus a higher oxidation state of alkane SOA in general. In this manner, the dihydrofuran chemistry can be considered as a "dehydration" channel in alkane SOA formation.

Supplementary material related to this article is available online at http://www.atmos-chem-phys-discuss.net/13/24713/2013/ acpd-13-24713-2013-supplement.pdf.

Acknowledgements. This work was supported by National Science Foundation grant AGS-1057183.

ACPD
13, 24713–24754, 2013

References

Aiken, A. C., DeCarlo, P. F., and Jimenez, J. L.: Elemental analysis of organic species with electron ionization high-resolution mass spectrometry, Anal. Chem., 79, 8350–8358, doi:10.1021/ac071150w, 2007.

Aiken, A. C., Decarlo, P. F., Kroll, J. H., Worsnop, D. R., Huffman, J. A., Docherty, K. S., Ulbrich, I. M., Mohr, C., Kimmel, J. R., Sueper, D., Sun, Y., Zhang, Q., Trimborn, A., Northway, M., Ziemann, P. J., Canagaratna, M. R., Onasch, T. B., Alfarra, M. R., Prevot, A. S. H., Dommen, J., Duplissy, J., Metzger, A., Baltensperger, U., and Jimenez, J. L.: O/C and OM/OC ratios of primary, secondary, and ambient organic aerosols with high-resolution time-of-flight aerosol mass spectrometry, Environ. Sci. Technol., 42, 4478–4485, 2008.

Alfarra, M. R., Coe, H., Allan, J. D., Bower, K. N., Boudries, H., Canagaratna, M. R., Jimenez, J. L., Jayne, J. T., Garforth, A. A., Li, S. M., and Worsnop, D. R.: Characterization of urban and rural organic particulate in the lower Fraser valley using two Aerodyne aerosol mass spectrometers, Atmos. Environ., 38, 5745–5758, 2004.

Arey, J., Aschmann, S. M., Kwok, E. S. C., and Atkinson, R.: Alkyl nitrate, hydroxyalkyl nitrate, and hydroxycarbonyl formation from the NO_x-air photooxidations of C_5-C_8 *n*-alkanes, J. Phys. Chem. A., 105, 1020–1027, 2001

Atkinson, R., Arey, J., and Aschmann, S. M.: Atmospheric chemistry of alkanes: review and recent developments, Atmos. Environ., 42, 5859–5871, 2008.

Aumont, B., Valorso, R., Mouchel-Vallon, C., Camredon, M., Lee-Taylor, J., and Madronich, S.: Modeling SOA formation from the oxidation of intermediate volatility *n*-alkanes, Atmos. Chem. Phys., 12, 7577–7589, doi:10.5194/acp-12-7577-2012, 2012.

Aumont, B., Camredon, M., Mouchel-Vallon, C., La, S., Ouzebidour, F., Valorso, R., Lee-Taylor, J., and Madronich, S.: Modeling the influence of alkane molecular structure on secondary organic aerosol formation, Faraday Discuss., 165, 1–16, 2013.

Bloss, C., Wagner, V., Jenkin, M. E., Volkamer, R., Bloss, W. J., Lee, J. D., Heard, D. E., Wirtz, K., Martin-Reviejo, M., Rea, G., Wenger, J. C., and Pilling, M. J.: Development of a detailed chemical mechanism (MCMv3.1) for the atmospheric oxidation of aromatic hydrocarbons, Atmos. Chem. Phys., 5, 641–664, doi:10.5194/acp-5-641-2005, 2005.

Canagaratna, M. R., Jayne, J. T., Jimenez, J. L., Allan, J. D., Alfarra, M. R., Zhang, Q., Onasch, T. B., Drewnick, F., Coe, H., Middlebrook, A., Delia, A., Williams, L. R., Trimborn, A. M., Northway, M. J., DeCarlo, P. F., Kolb, C. E., Davidovits, P., and Worsnop, D. R.:

Chemical and microphysical characterization of ambient aerosols with the Aerodyne aerosol mass spectrometer, Mass Spectrom. Rev., 26, 185–222, 2007.
Cappa, C. D., Zhang, X., Loza, C. L., Craven, J. S., Yee, L. D., and Seinfeld, J. H.: Application of the Statistical Oxidation Model (SOM) to Secondary Organic Aerosol formation from photooxidation of C_{12} alkanes, Atmos. Chem. Phys., 13, 1591–1606, doi:10.5194/acp-13-1591-2013, 2013.
Cavalli, F., Barnes, I., and Becker, K. H.: FTIR kinetic, product, and modeling study of the OH-initiated oxidation of 1-butanol in air, Environ. Sci. Technol., 36, 1263–1270, 2000.
Chhabra, P. S., Ng, N. L., Canagaratna, M. R., Corrigan, A. L., Russell, L. M., Worsnop, D. R., Flagan, R. C., and Seinfeld, J. H.: Elemental composition and oxidation of chamber organic aerosol, Atmos. Chem. Phys., 11, 8827–8845, doi:10.5194/acp-11-8827-2011, 2011.
Craven, J. S., Yee, L. D., Ng, N. L., Canagaratna, M. R., Loza, C. L., Schilling, K. A., Yatavelli, R. L. N., Thornton, J. A., Ziemann, P. J., Flagan, R. C., and Seinfeld, J. H.: Analysis of secondary organic aerosol formation and aging using positive matrix factorization of high-resolution aerosol mass spectra: application to the dodecane low-NO_x system, Atmos. Chem. Phys., 12, 11795–11817, doi:10.5194/acp-12-11795-2012, 2012.
Crounse, J. D., McKinney, K. A., Kwan, A. J., and Wennberg, P. O.: Measurement of gas-phase hydroperoxides by chemical ionization mass spectrometry, Anal. Chem., 78, 6726–6732, 2006.
DeCarlo, P. F., Kimmel, J. R., Trimborn, A., Northway, M. J., Jayne, J. T., Aiken, A. C., Gonin, M., Fuhrer, K., Horvath, T., Docherty, K. S., Worsnop, D. R., and Jimenez, J. L.: Field-deployable, high-resolution, time-of-flight aerosol mass spectrometer, Anal. Chem., 78, 8281–8289, 2006.
Fraser, M. P., Cass, G. R., Simoneit, B. R. T., and Rasmussen, R. A.: Air quality model evaluation data for organics. 4. C_2–C_{36} non-aromatic hydrocarbons, Environ. Sci. Technol., 31, 2356–2367, 1997.
Gong, H. M., Matsunaga, A., and Ziemann, P. J.: Products and mechanism of secondary organic aerosol formation from reactions of linear alkenes with NO_3 radicals, J. Phys. Chem. A., 109, 4312–4324, 2005.
Hoekman, S. K.: Speciated measurements and calculated reactivities of vehicle exhaust emissions from conventional and reformulated gasolines, Environ. Sci. Technol., 26, 1206–1216, 1992.

ACPD
13, 24713–24754, 2013

Holt, T., Atkinson, R., and Arey, J.: Effect of water vapor concentration on the conversion of a series of 1,4-dydroxycarbonyls to dihydrofurans, J. Photochem. Photobiol. A: Chem., 176, 231–237, 2005.
Jenkin, M. E., Shallcross, D. E., and Harvey, J. H.: Development and application of a possible mechanism for the generation of cis-pinic acid from the ozonolysis of α- and β-pinene, Atmos. Environ., 34, 2837–2850, 2000.
Jenkin, M. E., Saunders, S. M., Wagner, V., and Pilling, M. J.: Protocol for the development of the Master Chemical Mechanism, MCM v3 (Part B): tropospheric degradation of aromatic volatile organic compounds, Atmos. Chem. Phys., 3, 181–193, doi:10.5194/acp-3-181-2003, 2003.
Jenkin, M. E.: Modelling the formation and composition of secondary organic aerosol from α- and β-pinene ozonolysis using MCM v3, Atmos. Chem. Phys., 4, 1741–1757, doi:10.5194/acp-4-1741-2004, 2004.
Jordan, C. E., Ziemann, P. J., Griffin, R. J., Lim, Y. B., Atkinson, R., and Arey, J.: Modeling SOA formation from OH reactions with C_8-C_{17} *n*-alkanes, Atmos. Environ., 42, 8015–8026, 2008.
Isaacman, G., Chan, A. W. H., Nah, T., Worton, D. R., Ruehl, C. R., Wilson, K. R., and Goldstein, A. H.: Heterogeneous OH oxidation of motor oil particles causes selective depletion of branched and less cyclic hydrocarbons, Environ. Sci. Technol., 46, 10632–10640, 2012.
Kirchstetter, T. W., Singer, B. C., Harley, R. A., Kendall, G. R., and Traverse, M.: Impact of California reformulated gasoline on motor vehicle emissions. 1. Mass emission rates, Environ. Sci. Technol., 33, 318–328, 1999.
Kleinman, L. I., Springston, S. R., Daum, P. H., Lee, Y.-N., Nunnermacker, L. J., Senum, G. I., Wang, J., Weinstein-Lloyd, J., Alexander, M. L., Hubbe, J., Ortega, J., Canagaratna, M. R., and Jayne, J.: The time evolution of aerosol composition over the Mexico City plateau, Atmos. Chem. Phys., 8, 1559–1575, doi:10.5194/acp-8-1559-2008, 2008.
Klotz, B., Barnes, I., and Imamura, T.: Product study of the gas-phase reactions of O_3, OH and NO_3 radicals with methyl vinyl ether, Phys. Chem. Chem. Phys., 6, 1725–1734, 2004.
Kroll, J. H., Smith, J. D., Che, D. L., Kessler, S. H., Worsnop, D. R., and Wilson, K. R.: Measurement of fragmentation and functionalization pathways in the heterogeneous oxidation of oxidized organic aerosol, Phys. Chem. Chem. Phys., 11, 8005–8014, 2009.
Lambe, A. T., Onasch, T. B., Croasdale, D. R., Wright, J. P., Martin, A. T., Franklin, J. P., Massoli, P., Kroll, J. H., Canagaratna, M. R., Brune, W. H., Worsnop, D. R., and Davidovits, P.: Transitions from functionalization to fragmentation reactions of laboratory secondary organic

ACPD
13, 24713–24754, 2013

aerosol (SOA) generated from the OH oxidation of alkanes precursors, Environ. Sci. Technol., 46, 5430–5437, 2012.
Lee, A. K. Y., Herckes, P., Leaitch, W. R., Macdonald, A. M., and Abbatt, J. P. D.: Aqueous OH oxidation of ambient organic aerosol and cloud water organics: formation of highly oxidized products, Geophys. Res. Lett., 38, L11805, doi:10.1029/2011GL047439, 2011.
Lim, Y. B. and Ziemann, P. J.: Products and mechanism of secondary organic aerosol formation from reactions of n-alkanes with OH radicals in the presence of NO_x, Environ. Sci. Technol., 39, 9229–9236, 2005.
Lim, Y. B. and Ziemann, P. J.: Effects of molecular structure on aerosol yields from OH radical-initiated reactions of linear, branched, and cyclic alkanes in the presence of NO_x, Environ. Sci. Technol., 43, 2328–2334, 2009a.
Lim, Y. B. and Ziemann, P. J.: Chemistry of secondary organic aerosol formation from OH radical-initiated reactions of linear, branched, and cyclic alkanes in the presence of NO_x, Aero. Sci. Technol., 43, 604–619, 2009b.
Lim, Y. B. and Ziemann, P. J.: Kinetics of the heterogeneous conversion of 1,4-hydroxycarbonyls to cyclic hemiacetals and dihydrofurans on organic aerosol particles, Phys. Chem. Chem. Phys., 11, 8029–8039, 2009c.
Liu, S., Day, D. A., Shields, J. E., and Russell, L. M.: Ozone-driven daytime formation of secondary organic aerosol containing carboxylic acid groups and alkane groups, Atmos. Chem. Phys., 11, 8321–8341, doi:10.5194/acp-11-8321-2011, 2011.
Loza, C. L., Craven, J. S., Yee, L. D., Coggon, M. M., Schwantes, R. H., Shiraiwa, M., Zhang, X., Schilling, K. A., Ng, N. L., Canagaratna, M. R., Ziemann, P. J., Flagan, R. C., and Seinfeld, J. H.: Secondary organic aerosol yields of 12-carbon alkanes, Atmos. Chem. Phys. Discuss., 13, 20677–20727, doi:10.5194/acpd-13-20677-2013, 2013.
MathWorks, MATLAB, 2002.
Martin, P., Tuazon, E. C., Aschmann, S. M., Arey, J., and Atkinson, R.: Formation and atmospheric reaction of 4,5-dihydro-2-methylfuran, J. Phys. Chem. A, 106, 11492–11501, 2002.
Miracolo, M. A., Presto, A. A., Lambe, A. T., Hennigan, C. J., Donahue, N. M., Kroll, J. H., Worsnop, D. R., and Robinson, A. L.: Photooxidation of low-volatility organics found in motor vehicle emissions: production and chemical evolution of organic aerosol mass, Environ. Sci. Technol., 44, 1638–1643, 2010.
Miracolo, M. A., Hennigan, C. J., Ranjan, M., Nguyen, N. T., Gordon, T. D., Lipsky, E. M., Presto, A. A., Donahue, N. M., and Robinson, A. L.: Secondary aerosol formation from pho-

ACPD
13, 24713–24754, 2013

tochemical aging of aircraft exhaust in a smog chamber, Atmos. Chem. Phys., 11, 4135–4147, doi:10.5194/acp-11-4135-2011, 2011.

Ng, N. L., Canagaratna, M. R., Jimenez, J. L., Chhabra, P. S., Seinfeld, J. H., and Worsnop, D. R.: Changes in organic aerosol composition with aging inferred from aerosol mass spectra, Atmos. Chem. Phys., 11, 6465–6474, doi:10.5194/acp-11-6465-2011, 2011.

Ng, N. L., Canagaratna, M. R., Zhang, Q., Jimenez, J. L., Tian, J., Ulbrich, I. M., Kroll, J. H., Docherty, K. S., Chhabra, P. S., Bahreini, R., Murphy, S. M., Seinfeld, J. H., Hildebrandt, L., Donahue, N. M., DeCarlo, P. F., Lanz, V. A., Prévôt, A. S. H., Dinar, E., Rudich, Y., and Worsnop, D. R.: Organic aerosol components observed in Northern Hemispheric datasets from Aerosol Mass Spectrometry, Atmos. Chem. Phys., 10, 4625–4641, doi:10.5194/acp-10-4625-2010, 2010.

Odum, J. R., Hoffmann, T., Bowman, F., Collins, D., Flagan, R. C., and Seinfeld, J. H.: Gas/particle partitioning and secondary organic aerosol yields, Environ. Sci. Technol., 30, 2580–2585, 1996.

Pankow, J. F. and Asher, W. E.: SIMPOL.1: a simple group contribution method for predicting vapor pressures and enthalpies of vaporization of multifunctional organic compounds, Atmos. Chem. Phys., 8, 2773–2796, doi:10.5194/acp-8-2773-2008, 2008.

Paulot, F., Crounse, J. D., Kjaergaard, H. G., Kurten, A., St. Clair, J. M., Seinfeld, J. H., and Wennberg, P. O.: Unexpected epoxide formation in the gas-phase photooxidation of isoprene, Science, 325, 730–733, 2009.

Presto, A. A., Miracolo, M. A., Kroll, J. H., Worsnop, D. R., Robinson, A. L., and Donahue, N. M.: Intermediate-volatility organic compounds: a potential source of ambient oxidized organic aerosol, Environ. Sci. Technol. 43, 4744–4749, 2009.

Presto, A. A., Miracolo, M. A., Donahue, N. M., and Robinson, A. L.: Secondary organic aerosol formation from high-NOx photo-oxidation of low volatility precursors: *n*-alkanes, Environ. Sci. Technol. 44, 2029–2034, 2010.

Reisen, F., Aschmann, S. M., Atkinson, R., and Arey, J.: 1,4-Hydroxycarbonyl products of the OH radical initiated reactions of C_5–C_8 *n*-alkanes in the presence of NO, Environ. Sci. Technol., 39, 4447–4453, 2005.

Robinson, A. L., Donahue, N. M., Shrivastava, M. K., Weitkamp, E. A., Sage, A. M., Grieshop, A. P., Lane, T. E., Pierce, J. R., and Pandis, S. N.: Rethinking organic aerosols: semivolatile emissions and photochemical aging, Science, 315, 1259–1262, 2007.

Russell, L. M., Bahadur, R., and Ziemann, P. J.: Identifying organic aerosol soures by comparing functional group composition in chamber and atmospheric particles, Proc. Natl. Acad. Sci., 108, 3516–3521, 2011.

Sadezky, A., Chaimbault, P., Mellouki, A., Römpp, A., Winterhalter, R., Le Bras, G., and Moortgat, G. K.: Formation of secondary organic aerosol and oligomers from the ozonolysis of enol ethers, Atmos. Chem. Phys., 6, 5009–5024, doi:10.5194/acp-6-5009-2006, 2006.

Sander, S. P., Abbatt, J., Barker, J. R., Burkholder, J. B., Friedl, R. R., Golden, D. M., Huie, R. E., Kolb, C. E., Kurylo, M. J., Moortgat, G. K., Orkin, V. L., and Wine, P. H.: Chemical kinetics and photochemical data for use in atmospheric studies, Evaluation No. 17. JPL Publication 10-6, Jet Propulsion Laboratory, Pasadena, available at: http://jpldataeval.jpl.nasa.gov, 2011.

Saunders, S. M., Jenkin, M. E., Derwent, R. G., and Pilling, M. J.: Protocol for the development of the Master Chemical Mechanism, MCM v3 (Part A): tropospheric degradation of non-aromatic volatile organic compounds, Atmos. Chem. Phys., 3, 161–180, doi:10.5194/acp-3-161-2003, 2003.

Schauer, J. J., Kleeman, M. J., Gass, G. R., and Simoneit, B. R. T.: Measurement of emissions from air pollution sources. 5. C_1–C_{32} organic compounds from gasoline-powered motor vehicles, Environ. Sci. Technol., 33, 1578–1587, 1999.

St. Clair, J. M., McCabe, D. C., Crounse, J. D., Steiner, U., and Wennberg, P. O.: Chemical ionization tandem mass spectrometer for the in situ measurement of methyl hydrogen peroxide, Rev. Sci. Instrum., 81, 094102, doi:10.1063/1.3480552, 2010.

Thiault, G., Thévenet, R., Mellouki, A., and Le Bras, G.: OH and O_3 initiated oxidation of ethyl vinyl ether, Phys. Chem. Chem. Phys., 4, 613–619, 2002.

Tkacik, D. S., Presto, A. A., Donahue, N. M., and Robinson, A. M.: Secondary organic aerosol formation from intermediate-volatility organic compounds: cyclic, linear, and branched alkanes, Environ., Sci., Technol., 46, 8773–8781, 2012.

Yee, L. D., Craven, J. S., Loza, C. L., Schilling, K. A., Ng, N. L., Canagaratna, M. R., Ziemann, P. J., Flagan, R. C., and Seinfeld, J. H.: Secondary organic aerosol formation from Low-NO_x photooxidation of dodecane: evolution of multi-generation gas-phase chemistry and aerosol composition, J. Phys. Chem. A, 116, 6211–6230, 2012.

Zhang, X. and Seinfeld, J. H.: A functional group oxidation model (FGOM) for SOA formation and aging, Atmos. Chem. Phys., 13, 5907–5926, doi:10.5194/acp-13-5907-2013, 2013.

ACPD
13, 24713–24754, 2013

Zielinska, B., Sagebiel, J. C., Harshfield, G., Gertler, A. W., and Pierson, W. R.: Volatile organic compounds up to C_{20} emitted from motor vehicles, measurement methods, Atmos. Environ., 30, 2269–2286, 1996.

Ziemann, P. J. and Atkinson, R.: Kinetics, products, and mechanisms of secondary organic aerosol formation, Chem. Soc. Rev., 41, 6582–6605, 2012.

ACPD
13, 24713–24754, 2013

Table 1. Experimental conditions for the photooxidation of dodecane.

	Exp.	T (K)	RH (%)	HC (ppb)	(NO) (ppb)	(NO_2) (ppb)	(O_3) (ppb)	Initial Seed vol. ($\mu m^3\,cm^{-3}$)	Additional NO inj. ($ppb\,h^{-1}$) × (h)
High-NO_x[a]	1	~ 300	~ 3	208	430	576	< DL[g]	18	–
	2	~ 300	~ 3	208	287	12	~ 2	24	Y[c]
	3	~ 300	~ 11	206	45	33	~ 2	30	Y[d]
	4	~ 300	~ 20	178	38	156	~ 2	28	Y[e]
	5	~ 300	~ 55	214	69	30	~ 2	43	Y[f]
Low-NO_x[b]	6	~ 300	~ 3	208	< DL	< DL	< DL	19	–
	7	~ 300	~ 3	214	< DL	< DL	32.6	25	–
	8	~ 300	~ 55	216	< DL	< DL	< DL	58	–

[a] Under high-NO_x conditions, the simulated NO concentration (> 5 ppb) is at least four orders of magnitude higher than RO_2 (< 5×10^7 molecules cm^{-3}). Over 99 % of RO_2 is predicted to react with NO.
[b] Under low-NO_x conditions, the simulated HO_2 concentration (~ 1×10^{10} molecules cm^{-3}) is ~ 20 times higher than RO_2 (~ 5×10^8 molecules cm^{-3}). RO_2 + HO_2 dominates the fate of RO_2.
[c] NO source was controlled at 100 ppb h^{-1} for the first 7 h reaction and then 25 ppb h^{-1} for the remainder of the reaction.
[d] NO source was controlled at 25 ppb h^{-1} over the course of the experiment.
[e] NO source was controlled at 30 ppb h^{-1} for the first 3 h reaction and then 100 ppb h^{-1} for the next 1 h of reaction and then back to 30 ppb h^{-1} for the remainder of the reaction.
[f] NO source was controlled at 50 ppb h^{-1} over the course of the experiment.
[g] Detection limits (DL) for O_3, NO, and NO_2 are 0.5 ppb, 0.4 ppb, and 0.4 ppb, respectively. H_2O_2 has an interference on the O_3 detection, increasing the O_3 monitor readout by ~ 2–3 ppb in the current study.

ACPD
13, 24713–24754, 2013

Table 2. Proposed structures for CIMS ions unique to the alkyl-substituted dihydrofuran chemistry. C and T indicate the cluster and transfer product, respectively. Commercial standards are not available.

Observed m/z	Product	Chemical formula	Proposed structure	Chemical pathway	Interference
183 (+)	T	$C_{12}H_{22}O$	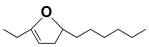	Heterogeneous conversion	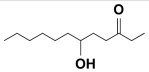
328 (−)	C	$C_{12}H_{21}NO_4$	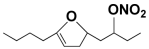	Heterogeneous conversion	–
346 (−)	C	$C_{12}H_{23}NO_5$	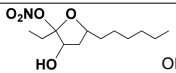	OH-oxidation	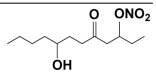
299 (−)	C	$C_{12}H_{22}O_3$	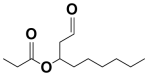	OH-oxidation Ozonolysis	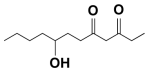
249 (−)	T	$C_{12}H_{22}O_4$	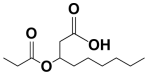	Ozonolysis	–
315 (−)	C	$C_{12}H_{22}O_4$	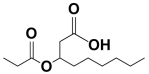	Ozonolysis	–
332 (−)	C	$C_{11}H_{21}O_5N$	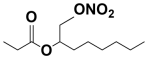	Ozonolysis	–
348 (−)	C	$C_{11}H_{21}O_6N$	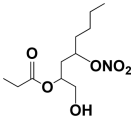	Ozonolysis	–
301 (−)	C	$C_{11}H_{20}O_4$	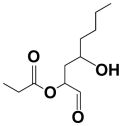	Ozonolysis	–

ACPD
13, 24713–24754, 2013

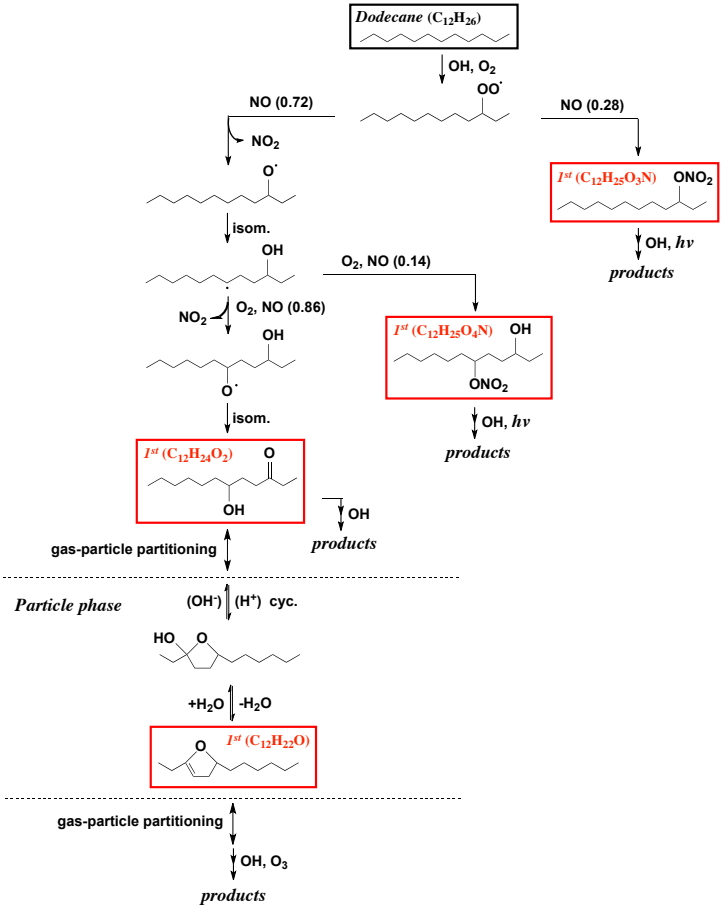

Fig. 1a. Schematic mechanism for the photooxidation of dodecane under high-NO_x conditions. Note only first-generation products are shown here. The solid color boxes indicate compounds and associated reaction pathways incorporated in the model simulation.

ACPD
13, 24713–24754, 2013

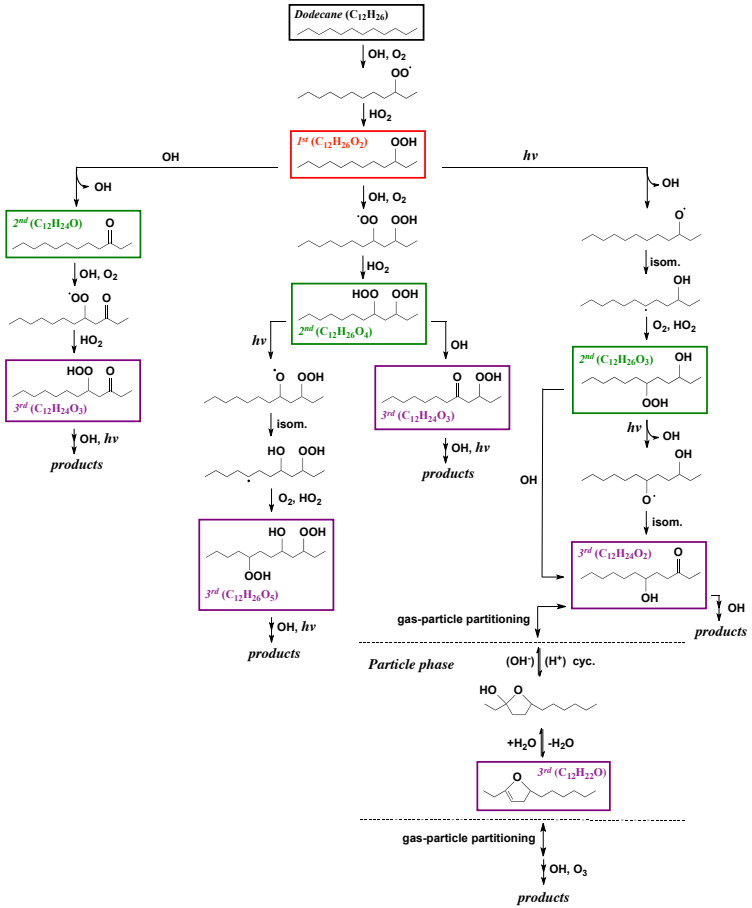

Fig. 1b. Schematic mechanism for the photooxidation of dodecane under low-NO_x conditions. Note only the first three generations of products are shown here. The solid color boxes indicate compounds and associated reaction pathways incorporated in the model simulation.

ACPD
13, 24713–24754, 2013

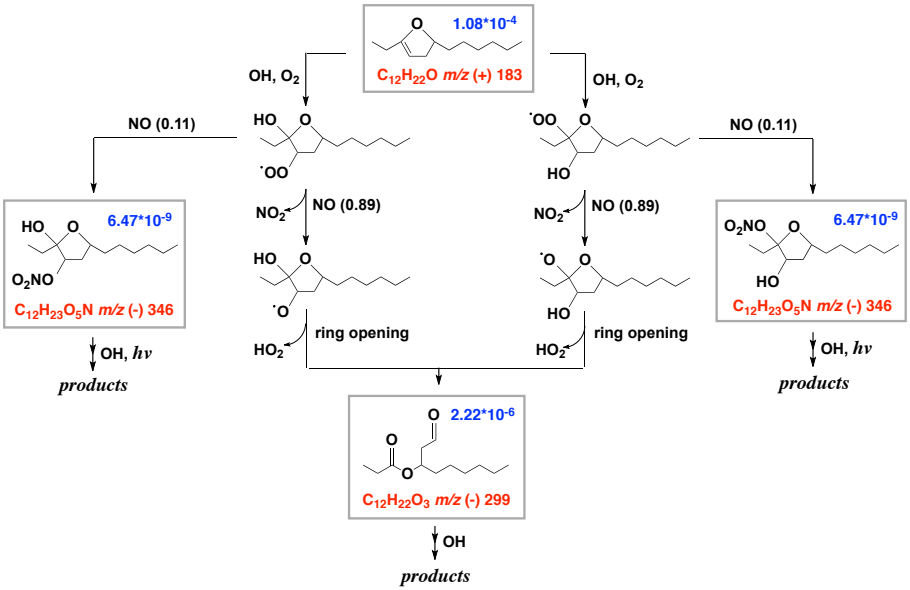

Fig. 2a. Proposed mechanism for the OH-initiated oxidation of alkyl-substituted dihydfrofuran under high-NO_x conditions. The solid gray boxes indicate compounds or reaction pathways incorporated in the model simulation. CIMS monitored species have m/z noted in red. Estimated vapor pressure (atm) of each compound is indicated in blue.

ACPD
13, 24713–24754, 2013

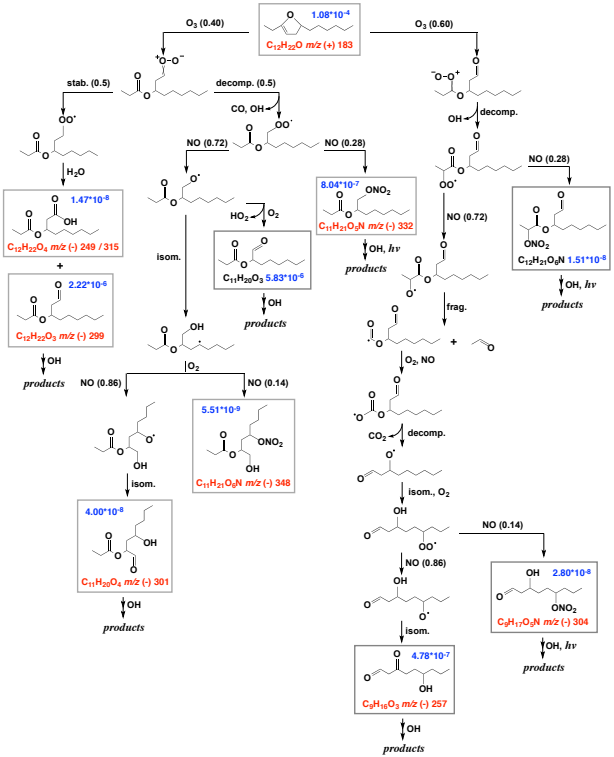

Fig. 2b. Proposed mechanism for the ozonolysis of alkyl-substituted dihydfrofuran under high-NO_x conditions. The solid gray boxes indicate compounds or reaction pathways incorporated in the model simulation. CIMS monitored species have m/z noted in red. Estimated vapor pressure (atm) of each compound is indicated in blue.

ACPD
13, 24713–24754, 2013

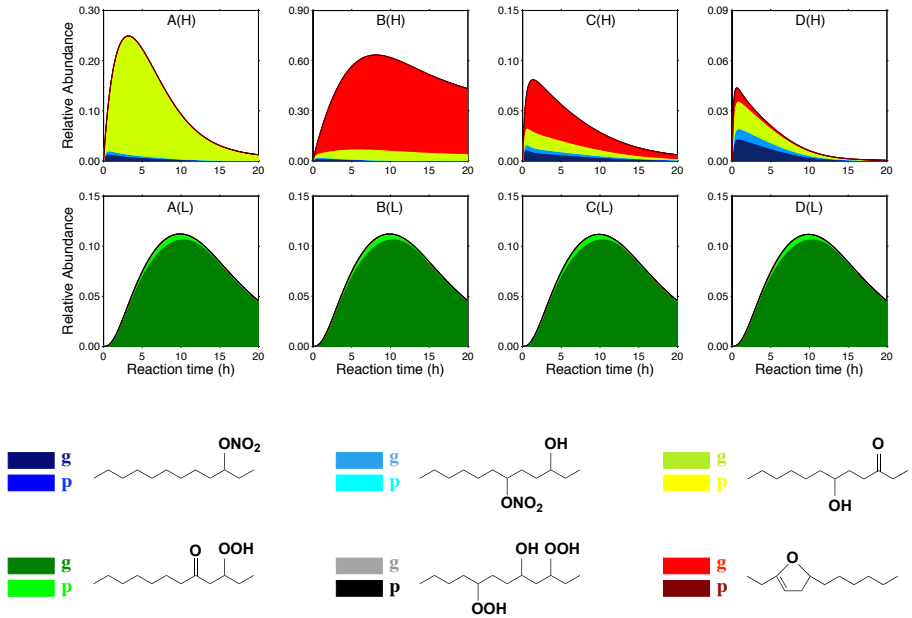

Fig. 3. Model-predicted relative abundance of δ-hydroxycarbonyl and alkyl-substituted dihydrofuran, together with other 1st generation products under high-NO_x (H) and other 3rd generation products under low-NO_x (L) conditions in gas (g) and particle (p) phases. All the organic masses are normalized by the initial organic mass (~ 200 ppb dodecane). (A) represents the relative abundance of products without a heterogeneous alkyl-substituted dihydrofuran formation channel; (B) represents the relative abundance of products when the heterogeneous channel is incorporated into the scheme but in the absence of any sink of alkyl-substituted dihydrofuran; (C) represents the relative abundance of products when the OH oxidation is the only sink of alkyl-substituted dihydrofuran; (D) represents the relative abundance of products using the complete gas- and particle- phase mechanism.

ACPD
13, 24713–24754, 2013

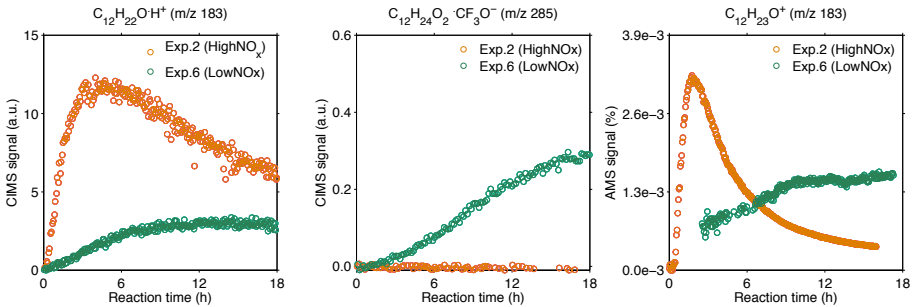

Fig. 4. Temporal profiles of ion $C_{12}H_{22}O{\cdot}H^+$ ($m/z = 183$) and $C_{12}H_{24}O_2{\cdot}CF_3O^-$ ($m/z = 285$) measured by CIMS and ion $C_{12}H_{23}O^+$ ($m/z = 183$) measured by AMS under high- and low-NO_x conditions. Details of experimental conditions are given in Table 1.

ACPD
13, 24713–24754, 2013

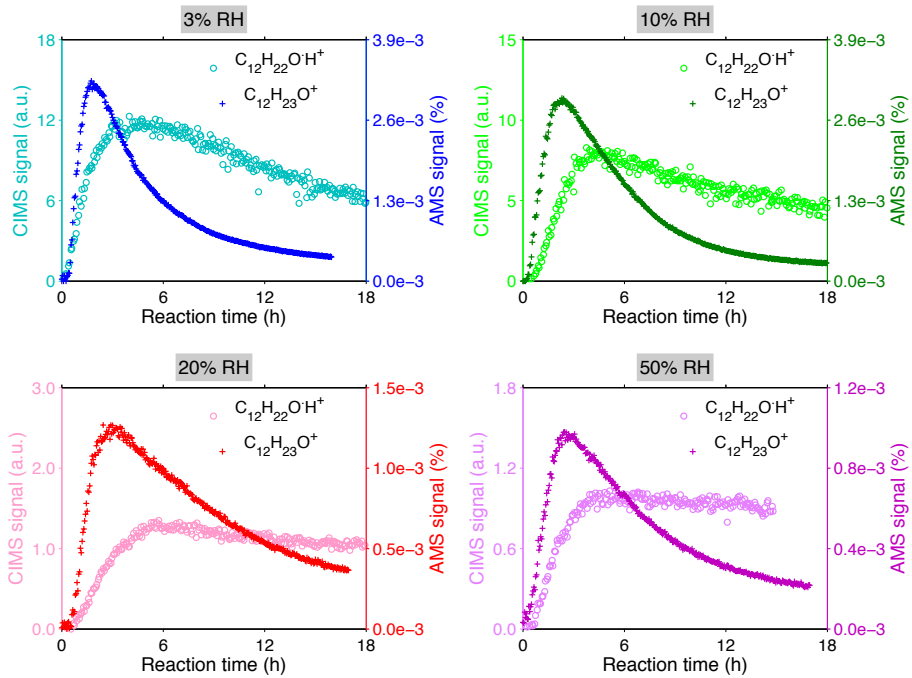

Fig. 5. Time-dependent evolution of ion $C_{12}H_{22}O{\cdot}H^+$ (m/z = 183) measured by CIMS and ion $C_{12}H_{23}O^+$ (m/z = 183) measured by AMS at 3 %, 10 %, 20 %, and 50 % RH.

ACPD
13, 24713–24754, 2013

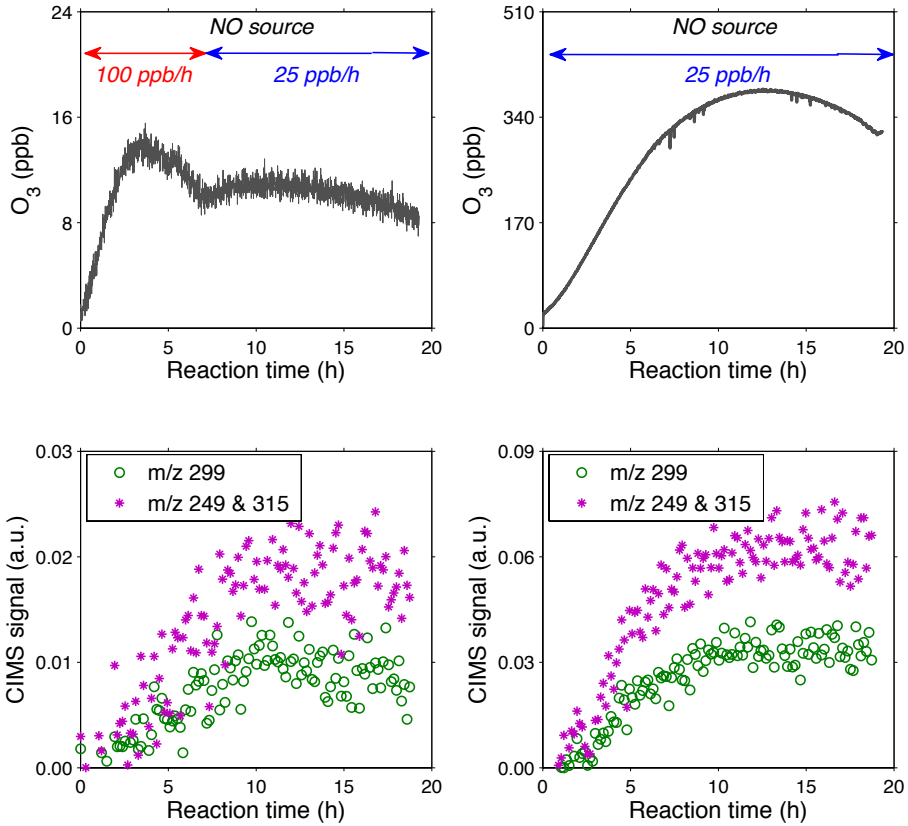

Fig. 6. Time-dependent evolution of CIMS detected signals m/z 299, and m/z 249 and 315, as a function of O_3 concentration over the course of 20 h photooxidation.

ACPD
13, 24713–24754, 2013

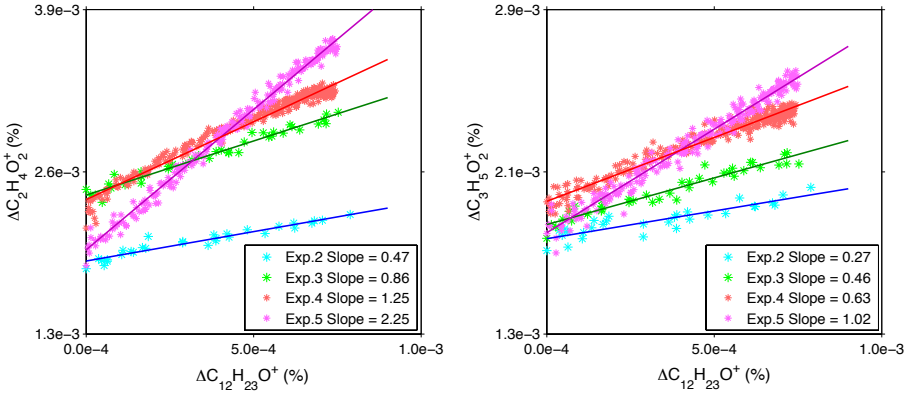

Fig. 7. Time-dependent evolution of AMS measured ion intensities of $C_2H_4O_2^+$ and $C_3H_5O_2^+$ as a function of decay of the $C_{12}H_{23}O^+$ signal.

ACPD
13, 24713–24754, 2013

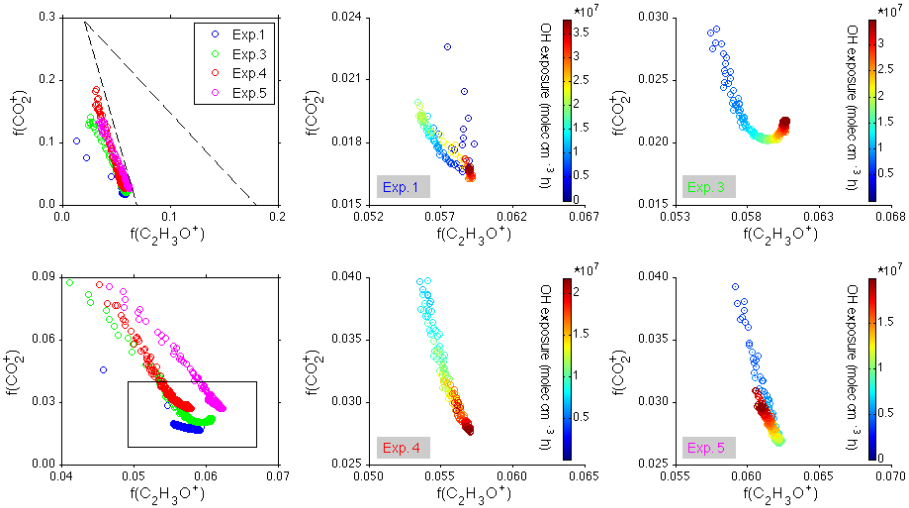

Fig. 8. SOA evolution as a function of OH exposure vs. O_3 exposure from dodecane photochemistry under high-NO_x conditions in the f_{44} vs. f_{43} space. The top-left graph shows the combination of all the data and the bottom-left graph shows a zoomed in version. The other graphs show the specific behavior of each experiment: Exp. 1 corresponds to a regime in which OH-oxidation of dihydrofuran is dominant. Exp. 3, 4, and 5 correspond to a regime in which ozonolysis of dihydrofuran is dominant, at 10 %, 20 %, and 50 % RH, respectively.

ACPD
13, 24713–24754, 2013

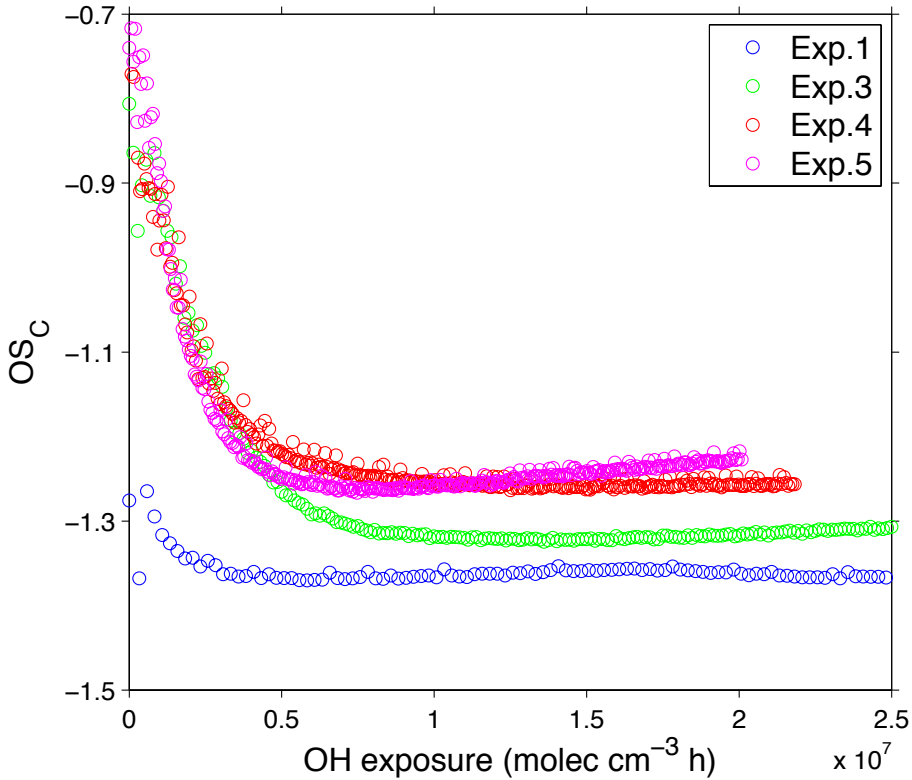

Fig. 9. SOA average carbon oxidation state as a function of OH exposure from dodecane photochemistry under high-NO_x conditions. Exp. 1 corresponds to a regime in which OH-oxidation of dihydrofuran is dominant. Exp. 3, 4, and 5 correspond to a regime in which ozonolysis of dihydrofuran is dominant, at 10 %, 20 %, and 50 % RH, respectively.

ACPD
13, 24713–24754, 2013

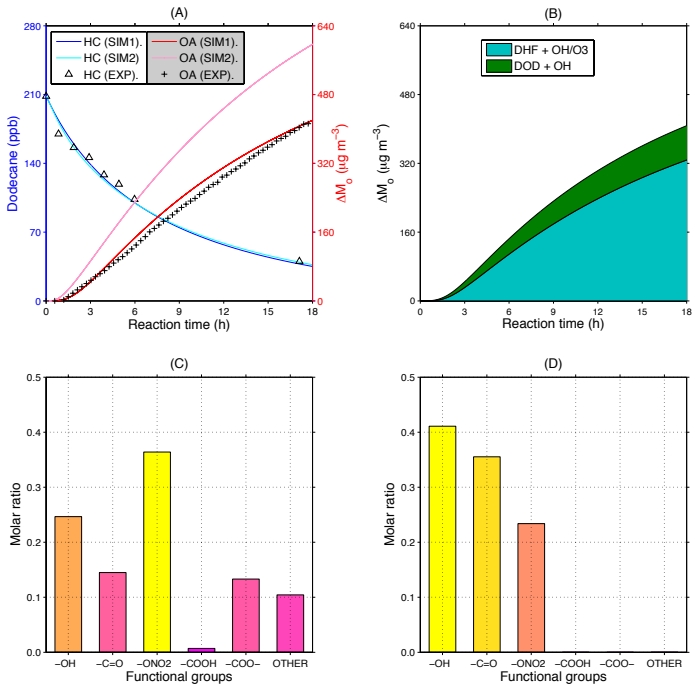

Fig. 10. (A) Comparison of the predicted dodecane decay and SOA growth with observations (Exp. #2). SIM1 represents the full mechanism simulations under initial conditions of Exp. #2. SIM2 is the simulations in the absence of the substituted dihydrofuran formation channel. **(B)** The contribution of dihydrofuran chemistry (DHF+OH/O_3) vs. dodecane photochemistry (DOD+OH) to the total organic mass. **(C)** Molar fractions of major functional groups after 3 h of photochemical reaction (when alkyl-substituted dihydrofuran peaks and organic loading is $\sim 50\,\mu g\,m^{-3}$) as predicted by SIM1. **(D)** Molar fractions of primary functional groups after 3 h of photochemical reaction as predicted by SIM2. Note that "other" includes dihydrofuran, tetrahydrofuran, and ether moieties.

ACPD
13, 24713–24754, 2013

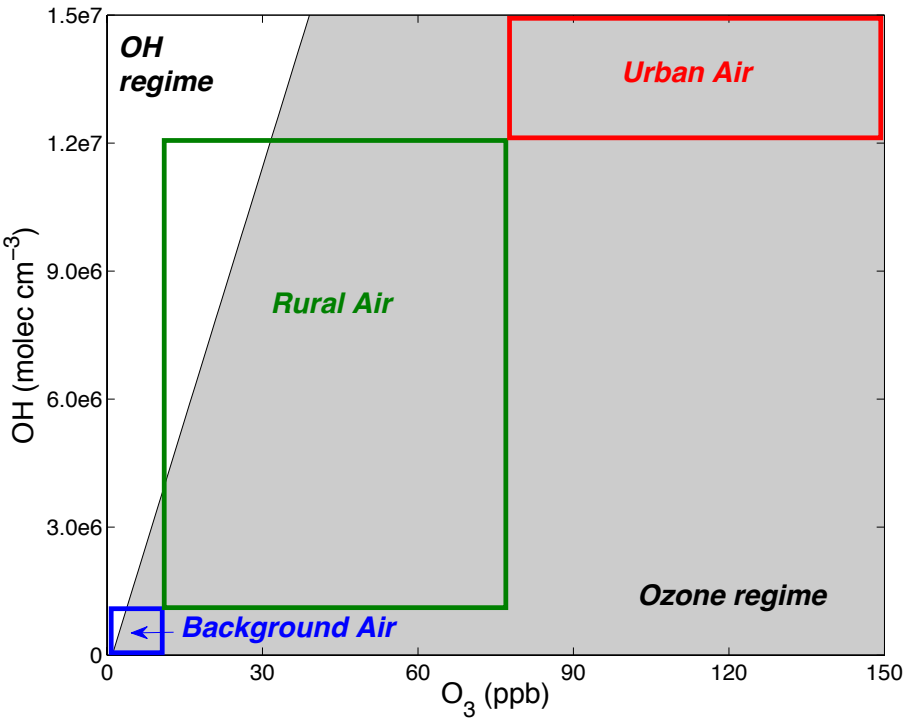

Fig. 11. Regimes of dominance of ozonolysis vs. OH-oxidation of substituted dihydrofuran. Daily maximum OH concentrations vary by regions in the troposphere, i.e., 10^5–10^6 molecules cm^{-3} for background air, 10^6–10^7 molecules cm^{-3} for rural air, and > 10^7 molecules cm^{-3} for urban air, with a global average concentration of 1×10^6 molecules cm^{-3}. Daily average surface ozone mixing ratios in rural areas are between 10 and 50 ppb, while these can exceed 100 ppb in polluted urban areas.

ACPD
13, 24713–24754, 2013